

This document was prepared in conjunction with work accomplished under Contract No. AT(07-2)-1 with the U.S. Department of Energy.

DISCLAIMER

This report was prepared as an account of work sponsored by an agency of the United States Government. Neither the United States Government nor any agency thereof, nor any of their employees, makes any warranty, express or implied, or assumes any legal liability or responsibility for the accuracy, completeness, or usefulness of any information, apparatus, product or process disclosed, or represents that its use would not infringe privately owned rights. Reference herein to any specific commercial product, process or service by trade name, trademark, manufacturer, or otherwise does not necessarily constitute or imply its endorsement, recommendation, or favoring by the United States Government or any agency thereof. The views and opinions of authors expressed herein do not necessarily state or reflect those of the United States Government or any agency thereof.

This report has been reproduced directly from the best available copy.

Available for sale to the public, in paper, from: U.S. Department of Commerce, National Technical Information Service, 5285 Port Royal Road, Springfield, VA 22161

phone: (800) 553-6847

fax: (703) 605-6900

email: orders@ntis.fedworld.gov

online ordering: <http://www.ntis.gov/support/index.html>

Available electronically at <http://www.osti.gov/bridge>

Available for a processing fee to U.S. Department of Energy and its contractors, in paper, from: U.S. Department of Energy, Office of Scientific and Technical Information, P.O. Box 62, Oak Ridge, TN 37831-0062

phone: (865)576-8401

fax: (865)576-5728

email: reports@adonis.osti.gov

DISTRIBUTION

F. E. Kruesi, Wilm
R. E. Naylor
S. Mirshak, SRP
J. R. Hilley
D. A. Ward
H. E. Wingo
B. S. Spangler
J. P. Morin
N. E. Barnett
C. H. Ice, SRL
J. L. Crandall
G. F. Merz
P. L. Roggenkamp

R. L. Frontroth
J. A. Smith
F. D. King
S. D. Harris
C. J. Temple
H. P. Olson
D. R. Muhlbaier
V. Whatley
E. L. Bryant
J. L. Steimke
TIS File
Vital Records

RECORD COPY

July 5, 1977

TO: G. F. MERZ

FROM: S. D. HARRIS-J. R. TAYLOR

SPRAY COOLING OF SIMULATED DROPPED IRRADIATED SLUG ASSEMBLIES

INTRODUCTION

A mechanism has been postulated for dropping an assembly containing slugs from the discharge machine during reactor discharge.⁽¹⁾ This memorandum provides calculational procedures and experimental bases for calculating maximum temperatures in a dropped slug assembly when it is being cooled by the existing emergency spray system.

SUMMARY

A spray system is available in the reactor room for cooling an assembly dropped during reactor discharge. Experimental work and calculations show that this system can provide sufficient cooling to prevent gross fission product release in a nominal Mark 31A assembly dropped onto the reactor room floor. For an assembly operating at its discharge power limit (29kw) and cooled by minimum measured spray density (0.2 gpm/ft²)*, calculated maximum inner slug temperature is 470°C. This compares to an experimentally determined limit of 700°C

*Maximum slug temperature is insensitive to spray density for spray densities above 0.13 gpm/ft² (Technical Standard Limit).

for gross release of fission products (reference 1).

Although the experimental work was done with Mark 31A geometry (Mark 31A is the only nested slug column operated at SRP at present), generalized calculational procedures are provided for analyzing other concentric geometries which are at least as massive.

Anomalies which could lead to higher calculated temperatures include:

- misshapen rib tips
- undersized slugs suspended between larger slugs (ribs on the smaller slug not in contact with the outer slug)

The probability of overheating as a result of these anomalies is small.

DISCUSSION

Background

A mechanism has been postulated for dropping an assembly containing slugs onto the reactor room floor from the discharge machine during reactor discharge.⁽¹⁾ An emergency spray system has been provided in the reactor room to cool such an assembly. Table I shows measured spray densities at various locations on the reactor room floor in P Area. Minimum spray density measured was 0.2 gpm/ft² (a minimum local spray density of 0.13 gpm/ft² in the crane operating area is required by standards).⁽²⁾ The spray system is periodically tested and adjusted if necessary to provide the spray pattern required.

If a slug assembly were dropped and inadequately cooled, it could melt and release fission products to the reactor room. For Mark 31 assemblies, the aluminum cladding could melt at temperatures as low as 577°C (because of silicon buildup during irradiation). However, the molten aluminum would alloy with the uranium core to form a brittle crust which would remain as an effective barrier to fission product release until the temperature exceeded 700°C.⁽¹⁾ Thus, sufficient cooling must be provided to limit metal temperatures in the assembly to 700°C.

Calculations for slug assemblies presently used at SRP⁽¹⁾ have shown that the existing spray system is adequate to prevent melting and fission product release for all assemblies. However, calculated cooling capability for a Mark 31A assembly was marginal. (Mark 31A is the most severe case because it is the only nested slug column presently used.) Calculated heat removal capability was based on data from the literature not directly applicable to SRP assemblies because test conditions did not duplicate conditions at SRP. An experimental program was undertaken to better define heat removal characteristics of the spray cooling system.

The experimental program consisted of separate test series to define:

- heat transfer between the water spray and the Mark 31A outer slug column

- internal heat transfer between inner slug column and outer slug column

The two separate test programs are discussed individually.

I. External Heat Transfer - Spray Cooling Outer Slug

Test Apparatus

The experimental apparatus used to study the interaction between the water spray and the assembly outer surface is shown in Figures 1, 2, and 3. The test assemblies were made from hollow stainless steel (Type 304) tubing with outside diameters of 1, 3, and 3.7 in. (Outside diameter of Mark 31A slugs is 3.7 in.) The tubes were electrically heated using the HTL rectifiers as a source of DC power. Electrical connections were made by bolting bus cables to steel plates welded to the tube 10 ft. apart, as shown in Figures 1 and 3. Less than 5% of total test section power was generated in the clamps.

The metal surface temperature was difficult to measure because of high electrical currents flowing through the tube. Type J (iron-constantan) thermocouples with insulated stainless steel sheaths were passed through 0.125-in. holes in one wall of the tube and pressed against the inside of the opposite wall. The thermocouples were bent slightly so that contact would be maintained as the tube expanded when heated. The thermocouples were fixed in place, and the entrance holes sealed with silver solder.

Four to six thermocouples were used on each tube. Two were placed in the center of the tube length, one of these at the top of the tube (nearest the spray nozzles) and one other on the side 90 degrees circumferentially away. The other four thermocouples were about 3 feet to each side of the central pair, one of each pair against the side of the tube and the second against the bottom of the tube. The thermocouples were far enough away from the bus connections to be in the area of uniform heat generation and also subject to the same spray density which tapered off slightly toward each end of the tube. Temperatures measured were corrected for the radial temperature gradient through the wall.

The spray system (Figure 2) consisted of a manifold with six nozzles spaced 24 in. apart. The first and last nozzles were directly above the bus connections of the test section. The system was intended to simulate as closely as possible the spray pattern that would be experienced by an assembly lying horizontally on the reactor room floor. The primary parameter of the spray was the spray density at the floor, with droplet size and droplet impact velocity held constant.

The spray density in the reactor process room is periodically measured by placing about 100 buckets uniformly around the reactor room floor, operating the spray system for a given time, and then recording the quantity of water in each bucket. By this method, a range of densities from 0.2 to 1.0 gal/(min-ft²) was measured. Nozzles in the laboratory mockup were selected to give the same range of spray densities at the floor as measured by the same technique. Qualitatively, these spray densities have an appearance ranging from a light rainfall to a very severe tropical thundershower. The

spray shown in Figure 3 was about 0.2 gal/min-ft^2 , the lower end of the range.

Three sets of nozzles made by Spraying Systems Company were used in the tests. The nozzles were designed to deliver a square spray pattern with good distribution throughout the square pattern. The spray cones overlapped when arranged in a row as shown in Figure 2, and delivered a reasonably uniform density along the length of the tube. Although each nozzle type could deliver spray at the full range of desired densities, use of three different sizes permitted each nozzle to be operated in a range to give nearly equal mean droplet velocities. Small nozzles were used for sprays less than 0.2 gpm/ft^2 , medium size for 0.2 to 0.4 gpm/ft^2 , and the largest nozzles for high spray rates. Droplet impact velocities were calculated to be typical for raindrop terminal velocities (20 to 30 ft/sec).

Total water flow to the nozzle manifold was measured with a calibrated metering orifice upstream of the manifold. Spray water temperature was measured with an iron-constantan thermocouple. Water temperature typically varied from 18 to 22°C during a test. Because room temperatures were in the same range, the analysis assumed that the spray water temperature just before impact was the same as that measured in the pipe: i.e., no heat transfer between air and water, and no evaporation in the fall from nozzle to floor.

Procedure

The procedure followed to obtain steady state heat transfer data consisted of establishing a known steady spray on a test cylinder, increasing the heat generation rate in steps, and recording metal temperatures when a steady state was attained when all metal temperatures remained constant for at least one minute. Total current flow and voltage drop across the tube were read and recorded for calculation of heat generation. Power was usually increased in steps of 10kw for each tube and spray rate.

At low powers, where indicated surface temperatures were well below 100°C , the entire tube was covered with a film of water, and the main cooling mechanism was by liquid film convection cooling. As heat generation increased and temperature approached 100°C , evaporation became more important, and with further increase in power, patches of the tube surface would briefly dry out and rewet, primarily on the underside of the tube. When one or more patches remained dry for too long, that area of the tube would heat up rapidly beyond the Leidenfrost point*, approximately 250°C ⁽³⁾, and become overheated. The test series for each spray rate was terminated when an area on the tube became red hot. The average wall temperature just beyond this dryout was usually 110 to 125°C .

For transient tests, the tube was heated at constant power to various initial surface temperatures before the spray was turned on. Typically

*The Leidenfrost point is the temperature at which a drop of water will no longer wet a surface.

the surface temperature continued to rise even after the spray was started; but after the surface was wetted by a water film, the temperature decreased rapidly toward a steady value equal to that for steady state tests at the same power and spray density. Wetting was rapid at initial surface temperatures below the Leidenfrost temperature, as would be expected. When the initial surface temperature was above the Leidenfrost temperature, spray cooling was ineffective, and tests were terminated so that the heater tubes would not be destroyed.

Data Analysis and Results

Steady State Tests

The primary heat transfer mechanism for cooling the steel tubes is liquid film cooling with evaporation on the tube surface. Overall heat transfer coefficient h was computed from the data according to the definition:

$$h = \frac{q/A}{(T_o - T_s)} \quad (1)$$

where q is the total heat generation; A , the total cylinder surface area between bus connections; T_o , the average outer surface temperature; and T_s , the spray water temperature. Outer tube surface temperature T_o is the arithmetic average of the thermocouple measurements, corrected for the temperature gradient through the tube wall with a solution to the one-dimensional heat conduction equation:

$$T_o - T_i = \dot{q} \frac{r_i^2}{2K_m} \ln \frac{r_o}{r_i} - \frac{\dot{q}}{4K_m} (r_o^2 - r_i^2) \quad (2)$$

Where \dot{q} is specific heat generation, pcu/ft^3 ; K_m is thermal conductivity of the metal. This calculation is based on no heat flux from inside wall of the tube. Heat transfer by radiation and convection from one section of the interior wall to another is calculated not to cause errors from this assumption greater than the overall experimental error of the data. As a further check, a thermocouple was positioned in the center of the 3-inch tube in one series of experiments to indicate inside air temperature. Air temperature always agreed with wall temperature within 3°C after steady state temperature was reached.

Generally, the measured surface temperatures agreed to within $\pm 10^\circ\text{C}$, with thermocouples in a pair usually agreeing to within $\pm 5^\circ\text{C}$. Observation of the spray density suggests that differences of $\pm 10^\circ\text{C}$ between pairs of thermocouples were due to variations in the spray density along the tube length rather than thermocouple errors or azimuthal location. At low powers, where cooling was entirely by liquid film, systematic differences between thermocouples on top, side, and bottom were apparent, with the topside thermocouples the

coolest. At higher powers, differences in thermocouple reading were erratic, and no azimuthal trend could be consistently discerned.

Figures 4, 5, and 6 show heat transfer coefficients plotted against averaged differences between tube surface and spray water temperature for various spray densities. The coefficient increases with spray density and temperature difference as expected. The Nusselt number (hD/k) calculated using the diameter of the cylinder and thermal conductivity of water, K , is plotted in Figure 7 against a parameter combining spray density and temperature difference:

$$\frac{SD T_o - T_s}{\nu T_{sat} - T_s} \quad (3)$$

where S is the spray density, D is the tube diameter, ν is the kinematic viscosity of water, and T_{sat} is the saturation temperature of the water (100°C in all of these tests). Curves representing data for the two larger tubes are close together whereas the 1 in. tube is considerably lower (Mark 31A outer diameter is 3.7 inches). Data were not obtained for tubes with diameters between 1 in. and 3 in.

The limited data suggests that the Nusselt number varies as $D^{3/4}$. The ratio of droplet spacing at impact to the tube diameter should be a factor in the large increase in heat transfer between the small tube and the larger ones. For given nozzles, spray pattern droplet spacing could be represented by some mean value, more or less fixed, so that increasing tube size would offer an increasing interception area. (The mean droplet spacing was not determined, but is estimated to be about 1 in.) The increase in heat transfer rate would not necessarily be linear because of complicating factors such as tube curvature and splatter from droplets striking the floor adjacent to the tube.

The uncertainty in the use of the curves in Figures 4 through 7 is indicated by the scatter plot of Figure 8, showing h derived from the basic data against h determined from the smoothed curves of the figures. For a spray system with characteristics similar to the one used, the probable error from predictions with these data is $\pm 20\%$.

Transient Tests

Figure 9 is representative of results of transient tests, in which the tube was heated at constant power to various initial temperatures before spraying began. The results indicate the Leidenfrost point is a reliable guide to the ability of the spray system to arrest the temperature rise. As shown in Figure 9, the tube was quickly cooled at 21, 29, and 40kw (total heat generation) when the spray was initiated at 200°C surface temperature, well below the Leidenfrost temperature

($257 \pm 10^\circ\text{C}$).⁽³⁾ Current procedures limit discharge power for Mark 31A to 29kw or less. If the sprays are turned on before the Mark 31A slug surface temperature exceeds 200°C the slugs will be quickly cooled.

Data at higher surface temperatures show some temperature overshoot before enough wetting occurred to provide satisfactory cooling. Rewetting occurred in patches, which slowly grew to cover the whole tube, first along the top where the spray impacted directly, then around toward the bottom. When the tube surface was pre-heated to 300°C , the water spray could not cool the tube. For the curve labeled 20kw in Figure 9, it first appeared that the tube would be cooled because patches of rewetting began to appear 1 to 2 min. after starting the sprays. However, the patches did not grow, and after 6 to 8 min. most of the tube reached 600°C . At 31kw and 300°C , the water spray did not wet the tube, and temperatures continued to rise. Higher spray densities were able to cool the tube at higher heat generation rates, but the initial surface temperature relative to the Leidenfrost temperature remained the determining factor.

II. Internal Heat Transfer - Inner to Outer Slug

Test Apparatus

A cross-section of the test assembly used to study heat transfer between inner and outer slugs for a horizontal Mark 31A is shown in Figure 10. The assembly consists of a stainless steel heater wrapped with fiberglass cloth and surrounded by a concentric slug column made of Mark 31A inner slug rejects. The slug column is housed inside a water jacket of the same inner diameter as a Mark 31A outer slug column. Tests were conducted in the Fabrication Laboratory, Building 773-A.

A schematic of the test section and instrumentation is shown in Figure 11. Electrical (DC) power was provided to the heater tube by a 900 ampere Lincoln welding generator. Current and voltage output from the welding generator were measured to obtain test section power. The test assembly itself was contained inside a stainless steel box to reduce any potential radioactivity release from the Mark 31A slugs. Negative pressure was maintained inside the box by means of a HEPA filtered vacuum cleaner.

Building hot water flowed into the water jacket where it was heated by the test assembly before being passed into the building storm sewer. Water flow was measured with a rotometer. Water outlet temperature from the test section was measured with an iron-constantan thermocouple placed just outside the containment box; outlet temperature varied from $\sim 55^\circ\text{C}$ - 75°C for the tests. Inlet temperature was measured at several times during the testing program at zero power and found to be constant for a given set of conditions within $\sim 0.3^\circ\text{C}$.*

Slug temperatures were measured during the tests by iron-constantan thermo-

*Inlet temperature was found to be a weak function of test section flow. Furthermore, building hot water temperature (and thus test inlet temperature) was reduced $\sim 10^\circ\text{C}$ part way through the test program as a means for reducing energy consumption.

couples peened into the top part of the slug cladding. The thermocouple signals were transmitted to calibrated Brown strip chart recorders for readout.

Procedure

Test procedure consisted of establishing a constant power input to the test section and measuring steady state flow and temperature. Because of the massive slugs, several hours were required to attain steady state for some of the tests. Measured flow and temperature difference for the coolant were used as an independent check on test section power. Energy balances were reasonably consistent for most of the tests.

Tests were run for the following conditions:

- Slugs with full ribs, oriented vertically
- Slugs with full ribs, oriented at 45° to the vertical
- Slugs with 45% of each rib removed*, oriented vertically

Raw data (including energy balances) are listed in Table 2. Inner to outer slug temperature differences are plotted against test section power in Figure 12. Outer slug temperature is taken as the average of inlet and outlet temperature in the water jacket. Average water jacket temperature was $\sim 60^{\circ}\text{C}$ for most of the tests and showed little variation compared to inner slug temperature.

Note that all the data in Figure 12 flatten out above 400°C inner/outer slug temperature difference. This corresponds to an inner slug temperature of around 460°C . Analysis of thermal expansion in a nominal Mark 31A inner slug shows that all ribs would expand into contact with the water jacket at a temperature of 465°C . Thus, the flattening of the data in Figure 12 is attributed to increased rib contact as a result of thermal expansion.

Data Analysis and Results

Heat is transferred from inner to outer slugs in a horizontal Mark 31A assembly by three mechanisms:

1. Conduction through spacer ribs
2. Conduction/convection through the air gap which separates the slugs.
3. Radiation

*Ribs are normally 5-1/2" long. For the part rib tests, two coupons (each 1-1/4" long) were removed from each rib on the slugs.

The largest contributor to total heat transfer is metal conduction through the spacer ribs. The largest resistance to heat flow through the spacer ribs is at the interface between the rib and the water jacket.

Because of the metal microstructure, the area of intimate, metal-to-metal contact is only a small fraction of the total interface area. Furthermore, metal-to-metal contact area (and thus effective heat transfer coefficient) is a fairly strong function of interface pressure and temperature. Test data were used to obtain the variation in interface heat transfer coefficient with inner slug temperature. The variation in heat transfer coefficient with interface pressure was not determined during the tests. Thus, test results should not be applied to inner slugs which are appreciably less massive than Mark 31A.

Tests were run with ribs oriented vertically and at 45° to the vertical to determine worst case conditions for heat transfer. The data (Figure 12) show no appreciable difference between the two cases. This is probably due to compensating effects from rib contact area and interface bearing pressure.

To determine heat transfer coefficient at the rib tips, the difference in heat transfer rates between slugs with full ribs and slugs with part ribs was analyzed. Summing up the contributions to heat transfer for the case with full ribs, gives:

$$Q_f = H_f A_f \Delta T_f + K_{air} \frac{\alpha_f}{D_f} \Delta T_f + h_f \alpha_f \Delta T_f + \sigma \alpha_f F_e F_A \left[\left(\frac{T_H}{100} \right)_f^4 - \left(\frac{T_C}{100} \right)_f^4 \right] \quad (4)$$

Where the first term is the contribution from rib conduction, the second is the contribution from air conduction, the third is the contribution from convection, and the last is the contribution from radiation.

A similar summation for heat transfer with part ribs gives:

$$Q_p = H_p A_p \Delta T_p + K_{air} \frac{\alpha_p}{D_p} \Delta T_p + h_p \alpha_p \Delta T_p + \sigma \alpha_p F_e F_A \left[\left(\frac{T_H}{100} \right)_p^4 - \left(\frac{T_C}{100} \right)_p^4 \right] \quad (5)$$

The notation used in equations (4) and (5) is:

- Q = total heat transferred, pcu/hr°C
- H = effective heat transfer coefficient for rib conduction, pcu/ft²-hr°C
- A = heat transfer area at rib tip, ft²
- K_{air} = thermal conductivity of air, pcu/ft-hr°C

- α = effective heat transfer area for air conduction, convection, or radiation,* ft²
 D = thickness of channel, ft
 h = heat transfer coefficient for natural convection, pcu/ft²-hr°C
 σ = Stephan-Boltzman constant, 1.0 pcu/ft²-°C⁴
 F_e = emissivity factor, dimensionless
 F_A = shape factor, dimensionless
 T_H = metal temperature in inner slug, °C
 T_C = average temperature of water jacket, °C
 ΔT = $T_H - T_C$, °C

Subscript f refers to heat transfer with full ribs and p refers to heat transfer with part ribs.

If data are taken at constant inner/outer slug temperature difference, then $\Delta T_f = \Delta T_p = \Delta T$ in equations (4) and (5). Furthermore, since T_C is nearly constant^p for all the tests,

$$\left[\left(\frac{T_H}{100} \right)_f^4 - \left(\frac{T_C}{100} \right)_f^4 \right] \approx \left[\left(\frac{T_H}{100} \right)_p^4 - \left(\frac{T_C}{100} \right)_p^4 \right]$$

With these assumptions, equations (4) and (5) can be solved for H_f to give:

$$H_f = H_p \frac{A_p}{A_f} + \frac{Q_f - Q_p}{\Delta T A_f} - \frac{K_{air}}{A_f} \left(\frac{\alpha_f}{D_f} - \frac{\alpha_p}{D_p} \right) - (h_f \alpha_f - h_p \alpha_p) - \sigma F_e F_A (\alpha_f - \alpha_p)$$

$$\frac{\left(\frac{T_H}{100} \right)_f^4 - \left(\frac{T_C}{100} \right)_f^4}{\Delta T A_f} \quad (6)$$

A detailed analysis using equation (6) has been made to determine the lower bound on H_f by minimizing positive terms on the right and maximizing negative terms. The analysis is based on the following assumptions:

- $H_p = H_f$. This gives the minimum possible value to the first term because increased bearing pressure (as a result of removing part of the ribs) makes $H_p > H_f$.

*Because the annulus is thin, effective heat transfer area is assumed the same for all modes of heat transfer other than rib conduction.

- $h_p = h_f$. This gives the maximum possible value to the fourth term. Actually, $h_p > h_f$ because the ribs inhibit natural convection patterns. The value for h is obtained from DG Standards.
- $F_e = F_A = 1.0$. This is the maximum theoretical value for these two parameters. A value of F_e equal to 1.0 is only possible for radiant exchange between two black bodies.
- $\left(\frac{T_c}{T_{oo}}\right)^4$ is neglected when compared to $\left(\frac{T_H}{T_{oo}}\right)^4$. This leads to a conservatism of $\sim 10\%$ on radiation heat transfer. However, because radiation is a small contributor to total heat transfer, the overall error is small.

The resulting values for heat transfer coefficient are shown in Figure 13 as a function of inner/outer slug temperature difference.

A reasonable upper bound on heat transfer coefficient at the rib tip can be calculated by assuming heat transfer by rib conduction only (i.e., the last three terms in equation (6) are set to zero). The resulting upper bound values are $\sim 13\%$ higher than recommended values based on the lower bound.

III. Application to SRP Assemblies

To calculate inner slug temperature for a dropped reactor assembly, it is necessary to correct for:

- Temperature gradients in a Mark 31A outer slug which could be greater than those in the water jacket.
- Aluminum oxide films which could be thicker on the reactor assembly than on the test assembly.

This section presents corrections for these two effects as well as a procedure for calculating inner slug temperature in a dropped Mark 31A assembly.

Temperature Distribution in the Outer Slug

Temperature gradients in a Mark 31A outer slug would be substantially higher than gradients in the water jacket used during the tests for inner/outer slug heat transfer. An analytic solution for the temperature in a clad Mark 31A outer slug is presented in Appendix A based on:

- No heat generation in the outer slug
- Total heat transferred through a single rib
- Constant temperature on the outer surface of the outer slug

Figure 14 shows maximum temperature (directly beneath the rib centerline) in the Mark 31A outer slug as a function of inner slug power based on the

calculations from Appendix A. At the discharge cooling limit (773 watt/ft in the inner slug), inner slug temperature could be 165°C higher than measured during the test.

Aluminum Oxide

Surface oxidation of the aluminum cladding in a reactor assembly could also result in higher resistance to heat flow through the ribs than measured during the tests. Although surface oxide thickness was not measured on the test assemblies, a conservative estimate of increased temperature has been made based on:

- No oxide film on the test assembly
- Maximum oxide thickness of 0.06 mils for an irradiated Mark 31A assembly*
- Thermal conductivity for the oxide of 1.25 pcu/ft-hr°C

Under these assumptions, the temperature drop across the oxide film (at the rib tip) is

$$\Delta T_{\text{oxide}} = 4.804 P_{\text{inner}} \quad (7)$$

Where:

P_{inner} = linear power density in inner slug column, kw/ft. Thus, at the discharge power limit (0.773 kw/ft generated in the inner slug), the temperature drop across the oxide film is a maximum of 3.7°C.

A Sample Problem

To illustrate use of the data, a sample problem is solved below:

Given: MK-31A OD = 3.7"

Power = 29kw

Axial peaking = 1.4

Maximum heat flux = 6030 pcu/hr-ft²

$T_{\text{spray}} = 0.2 \text{ gpm/ft}^2$

Required: Surface temperature and maximum internal temperature

*Based on oxide thickness in autoclave. This is the maximum during the irradiation.

Outer Slug Surface Temperature

The outer surface temperature may be estimated from the data of Figure 6 by the following procedure:

- Estimate T_{wall}
- Compute $(T_{wall} - T_{spray}) = \Delta T$
- Find h from data (Figure 6)
- Compute heat flux = $h \cdot \Delta T$
- Adjust estimated T_{wall} and repeat until calculated heat flux equals given heat flux.

Numerically,

<u>Est. T_{wall}</u>	<u>ΔT</u>	<u>h</u>	<u>q/A</u> calc	
100	75	93	6975	high
80	55	68	3740	low
90	65	79	5293	close
93	68	83	5644	closer
95	70	86	6020	Close enough

Therefore, T_{wall} is 95°C. This value will be used to compute the maximum internal temperature.

Inner Slug Temperature

Maximum inner slug temperature for the Mark 31A assembly can be calculated from the equations below:

$$P_{inner} = \frac{K_{air}}{302 \ln r_2/r_3} (T_{inner} - T_{IS}) + \frac{h_{rib} A_{rib}/L}{1896} (T_{inner} - T_{COR}) \quad (8)$$

$$T_{IS} = T_w + \frac{\dot{q}}{4K_m} (r_1^2 - r_2^2) - \frac{\dot{q} r_2^2}{2K_m^2} \ln r_1/r_2 \quad (9)$$

$$T_{COR} = T_{CL} + \Delta_{oxide} \quad (10)$$

where

\dot{q} = specific power in outer slug, pcu/ft²-hr

K_m = thermal conductivity of outer slug, pcu/ft hr °C

- r_1 = radius of outer surface, inner slug, ft
 r_2 = radius of inner surface, outer slug, ft
 r_3 = radius of outer surface, outer slug, ft
 T_w = average temperature of outer surface, outer slug, °C
 T_{IS} = average temperature of inner surface, outer slug, °C
 T_{CL} = temperature beneath rib centerline (Figure 14), °C
 T_{COR} = centerline temperature corrected for oxide film, °C
 ΔT_{oxide} = temperature correction for oxide film - equation (7), °C
 T_{inner} = metal temperature in inner slug, °C
 h_{rib} = overall heat transfer coefficient for rib conduction (Figure 13),
 pcu/ft²-hr°C
 A_{rib} = heat transfer area at rib tip for contact by a single rib, ft²
 L = assembly length, ft
 K_{air} = thermal conductivity of air, pcu/ft-hr°C
 P_{inner} = linear power density in inner slug column, kw/ft

No credit is taken in this analysis for heat transfer by radiation or by natural convection.

Appropriate numerical values for Mark 31A are:

- K_m = 17 pcu/ft² - hr °C
 r_1 = 3.70 in = 0.308 ft
 r_2 = 2.59 in = 0.216 ft
 r_3 = 2.22 in = 0.185 ft
 L = 13.08 ft
 K_{air} = 0.025 pcu/ft-hr°C

Furthermore, \dot{q} can be calculated from

$$\dot{q} = 1896 \cdot \frac{P_{outer}}{\pi(r_1^2 - r_2^2)}$$

where P_{outer} is the linear power density in the outer slug, kw/ft.

The value for A_{rib} is calculated assuming contact by a single rib on each slug.* Each rib on a slug is 0.060 inches wide by 5.5 inches long. Furthermore, there are 18 inner slugs per Mark 31A assembly. Thus,

$$A_{rib} = 18 \frac{0.060}{144} (5.5) = 0.0413 \text{ ft}^2$$

A step by step procedure for calculating T_{inner} follows:

- 1) Determine T_w from the previous section. (For this problem, T_w is 95°C).
- 2) Determine P_{inner} and P_{outer} corresponding to 29kw total assembly power. For end of cycle conditions, the inner slug generates 24.9% to total Mark 31A power and the outer slug 75.1%. Applying a factor of 1.4 for axial peaking gives:

$$P_{inner} = 0.773 \text{ kw/ft}$$

$$P_{outer} = 2.33 \text{ kw/ft}$$

- 3) Calculate T_{IS} from equation (9). For this problem $T_{IS} = 101^{\circ}\text{C}$.
- 4) Determine T_{CL} from Figure 14 at the appropriate value of P_{inner} . For this problem, P_{inner} is 0.773 kw/ft.

Thus,

$$T_{CL} = T_w + 165^{\circ}\text{C}$$

$$T_{CL} = 260^{\circ}\text{C}$$

- 5) Adjust T_{CL} for oxide film according to equation (10). For this problem $T_{COR} = 264^{\circ}\text{C}$.
- 6) Assume a value of T_{inner} .
- 7) Determine h_{rib} by entering Figure 13 at the assumed value of T_{inner} .
- 8) Calculate P_{inner} from equation (8) and compare to the given value (0.773 kw/ft from step 2).
- 9) Adjust guess on T_{inner} and repeat steps 7 through 9 until desired accuracy is obtained.

*This is not a conservatism but a necessary result of the way h_{rib} is defined.

The following table lists the results of several iterations for the problem posed:

<u>Iteration Number</u>	<u>Assumed T_{inner}</u>	<u>h</u>	<u>P_{inner}</u>
1	500	1730	0.893
2	400	1470	0.493
3	450	1600	0.682
4	470	1660	0.770

Calculated P_{inner} from iteration 4 agrees within 1% with the given value of 0.773 kw/ft. Thus, maximum inner slug temperature for the problem posed is 470°C.

Maximum slug temperatures for other discharge powers and spray densities are shown in Figure 15. Maximum slug temperature is relatively insensitive to spray density because the temperature drop from outer surface to spray is a small contributor to overall temperature drop.

Anomalous Assemblies

Tests were run with assemblies containing nominally shaped ribs (0.010" radius at tips). It is possible to postulate other rib shapes which would reduce heat transfer area for rib conduction and thus increase metal temperature. However, irradiation of such misshapen ribs is unlikely.

Another anomaly which could result in increased metal temperature is decreased rib circle diameter. Nominal diametral clearance between the inner slug ribs and the outer slug is 30 mils. However, because of fabrication tolerances, diametral clearance may be as much as 40 mils. Thus it is possible for an undersized slug to become suspended (on the inner housing) between two oversized slugs. For worst case tolerances, the undersized slug could reach 600°C before thermal expansion forced the ribs to contact the outer surface. This condition is unlikely because sagging of the aluminum inner housing would probably allow rib contact at much lower temperatures (the melting point for pure aluminum is ~660°C.)

Furthermore, in the unlikely event that cladding should melt (as the result of these or other anomalies), the molten aluminum would bridge the gap between inner and outer slugs and greatly enhance heat transfer. Thus clad melting, however unlikely, is inherently self limiting.

REFERENCES

1. H. P. Olson, Memorandum to J. M. Boswell, *Spray Cooling of Dropped Irradiated Assemblies*, DPST-74-366, June 10, 1974.
2. DPSOL 1804, *Test-Emergency Spray Water*.
3. M. Cumo, D. Pitimade, *On the Determination of the Leidenfrost Point with Sprays of Water and Low Boiling Organics*, ASME Paper 73-HT-19, 1973.
4. J. R. Taylor, *Logbook*, DPSTN-2554. Unclassified.
5. *CRC Standard Math Tables*, The Chemical Rubber Company, 16th Edition.



FIGURE 1. Test Section (3.0 in diameter) in Position Showing Electrical Connections and Thermocouples



FIGURE 2. Spray Nozzle Manifold, Located 10 ft Directly above the Test Section

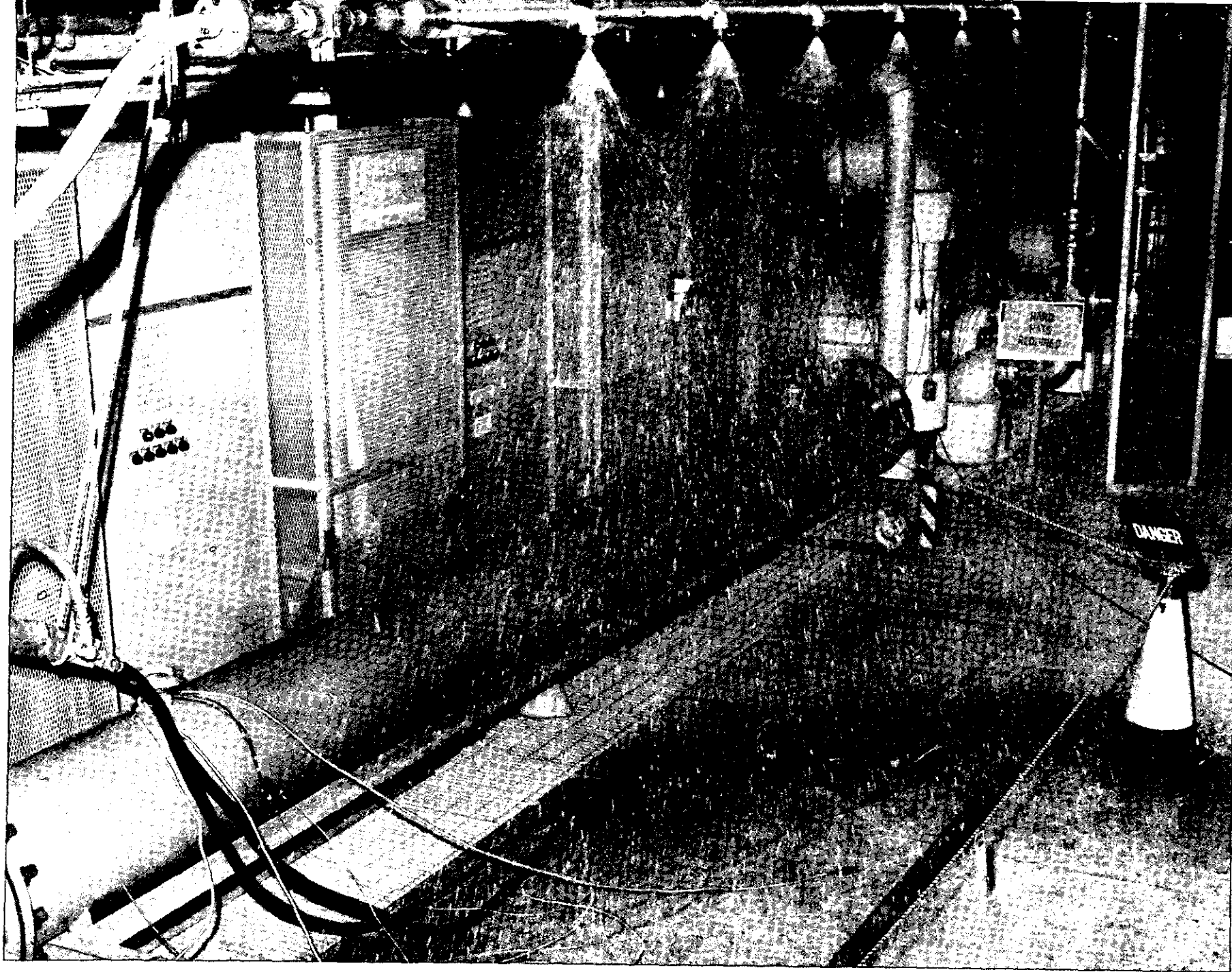


FIGURE 3. Complete Apparatus with Spray Cooling Water On

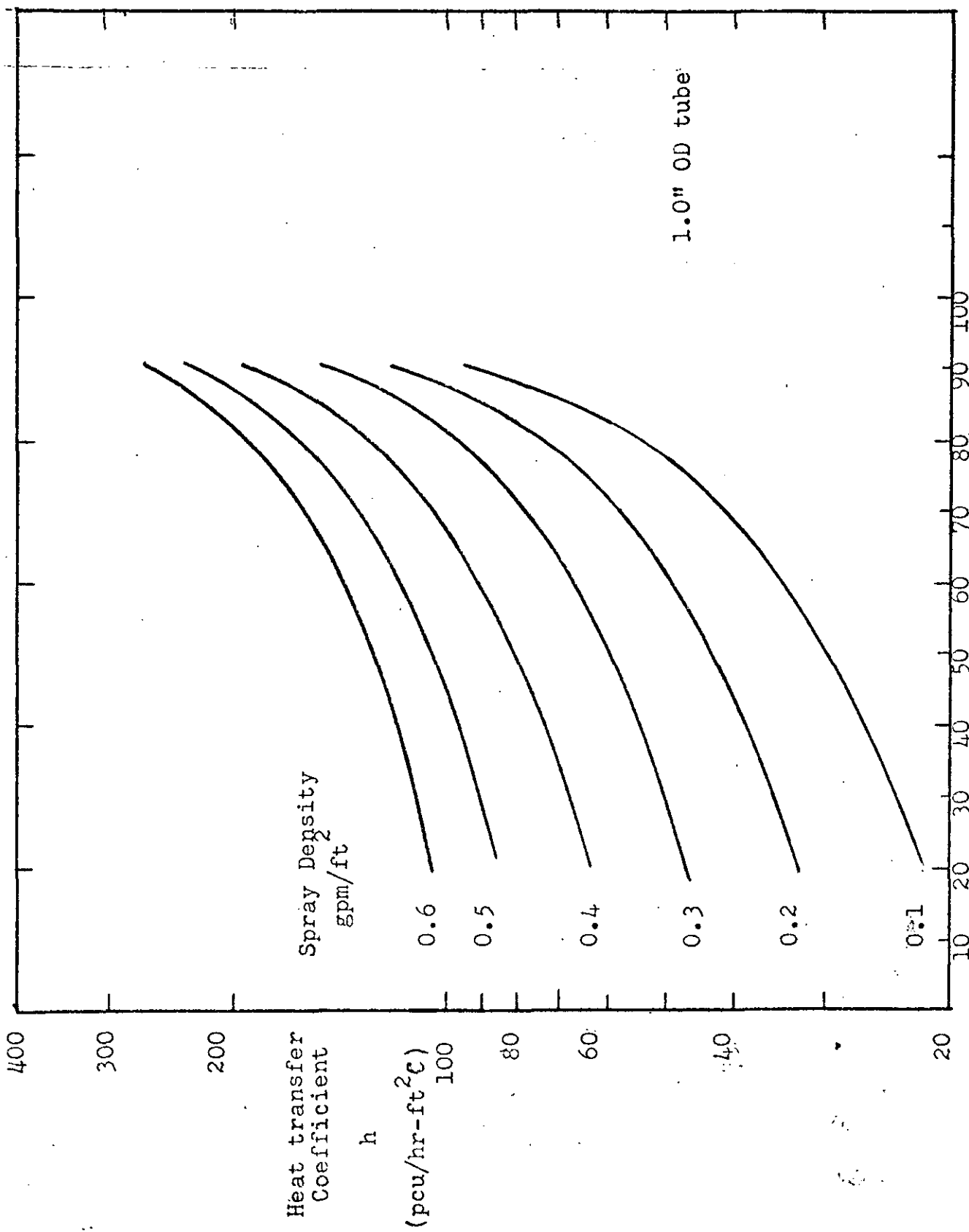


Figure 4. HEAT TRANSFER COEFFICIENT VS. TEMPERATURE DIFFERENCE FOR THE 1.00 in-DIAMETER TUBE

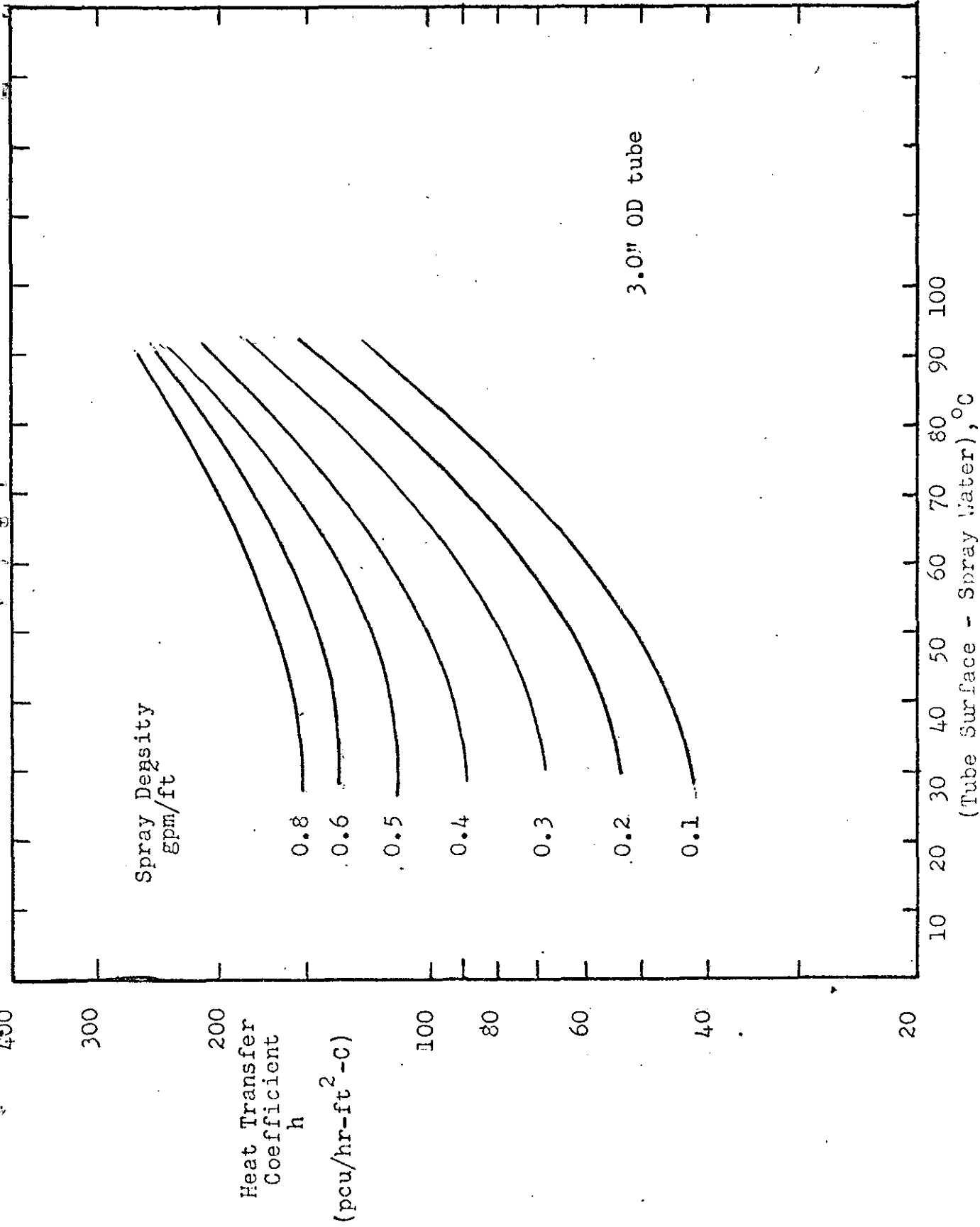
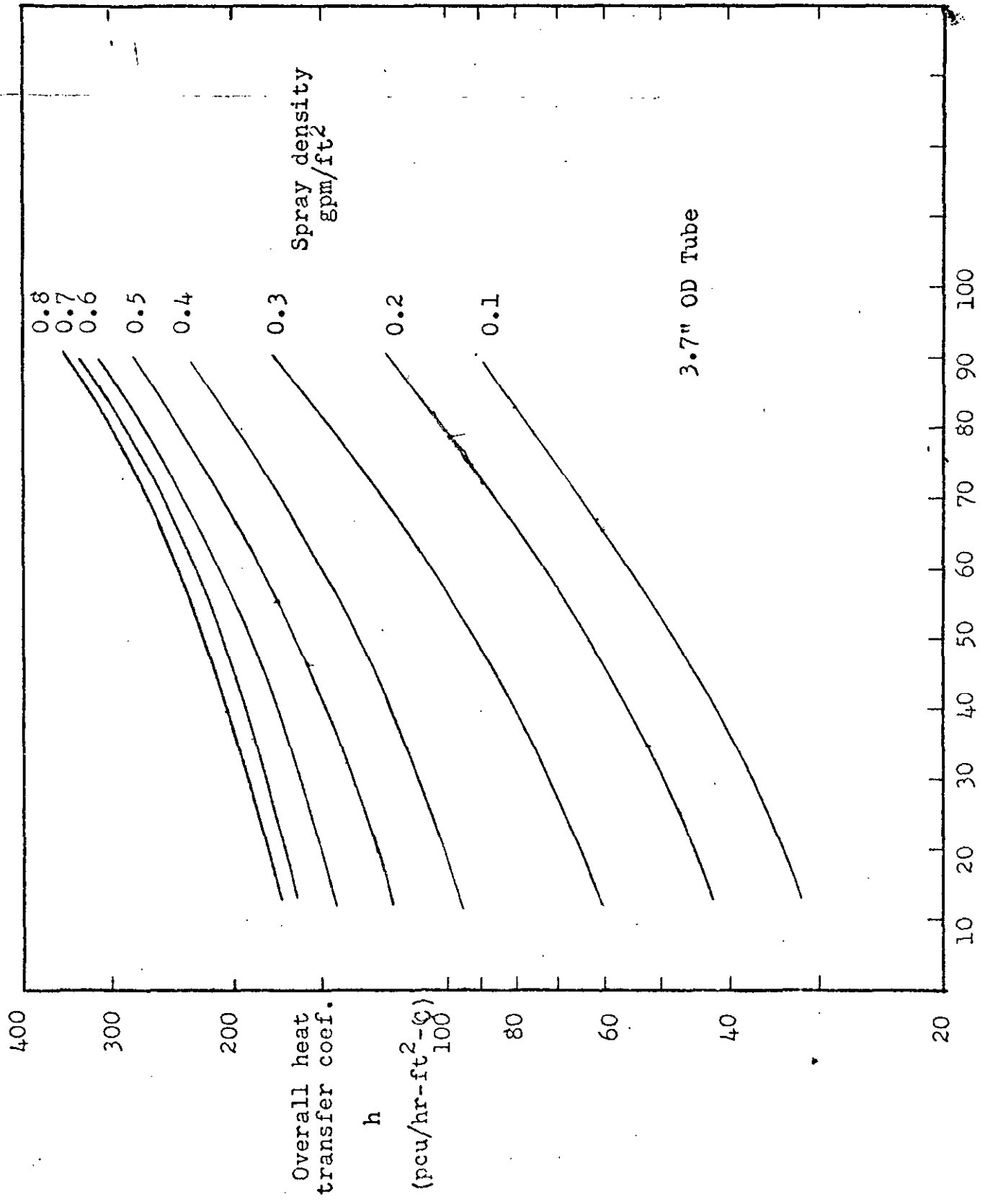


Figure 5. HEAT TRANSFER COEFFICIENT VS. TEMPERATURE DIFFERENCE FOR THE 3-INCH TUBE



Tube surface - Spray water temperature difference, C
Figure 6. HEAT TRANSFER COEFFICIENT VS. TEMPERATURE DIFFERENCE
FOR THE 3.7 INCH DIAMETER TUBE

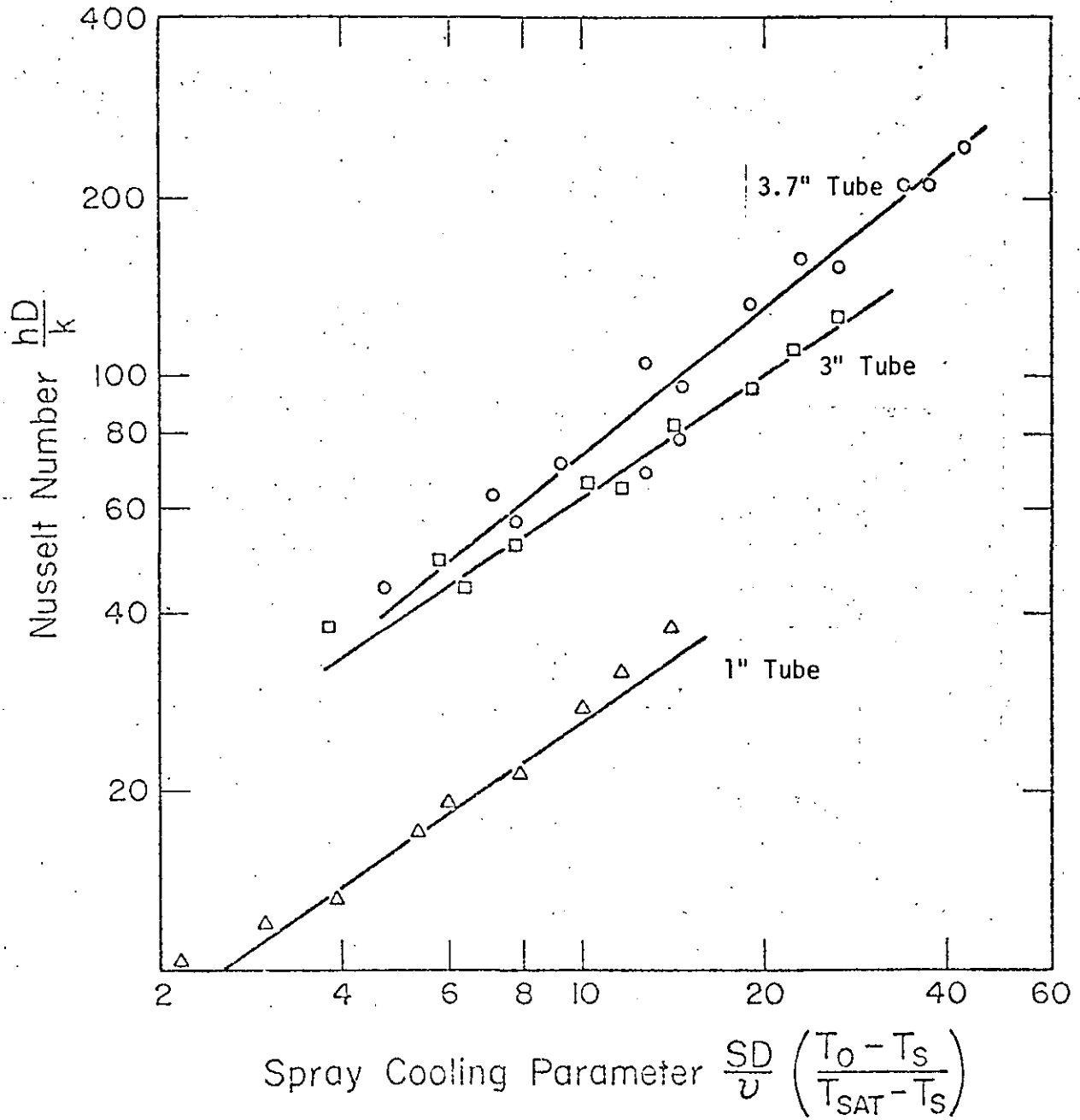


FIGURE 7. Nusselt Numbers for Spray Cooling, Showing Effect of Tube Diameter

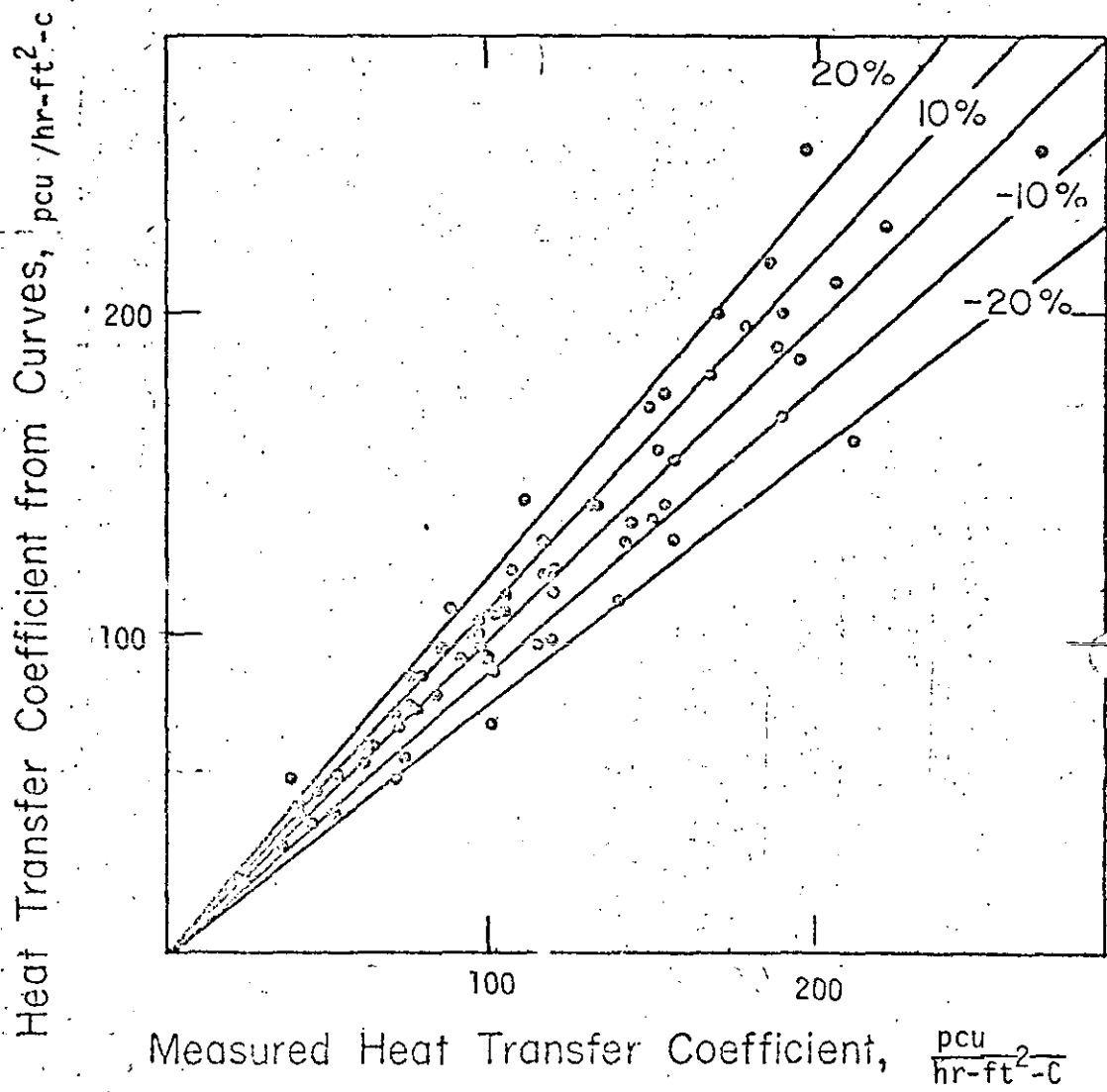


FIGURE 8. Measured Data for Heat Transfer Coefficients Compared to Coefficients Read from Smoothed Data Curves

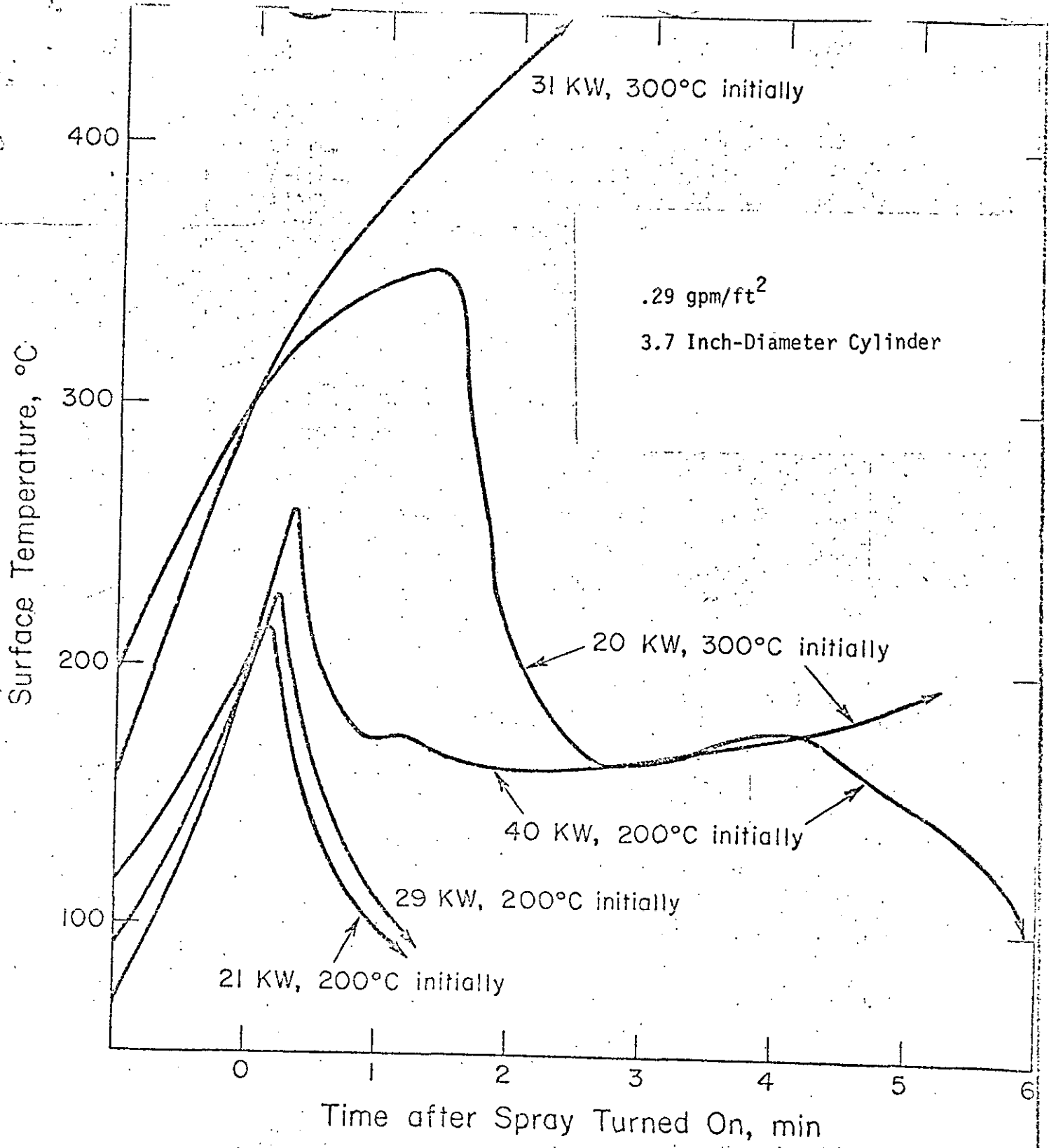
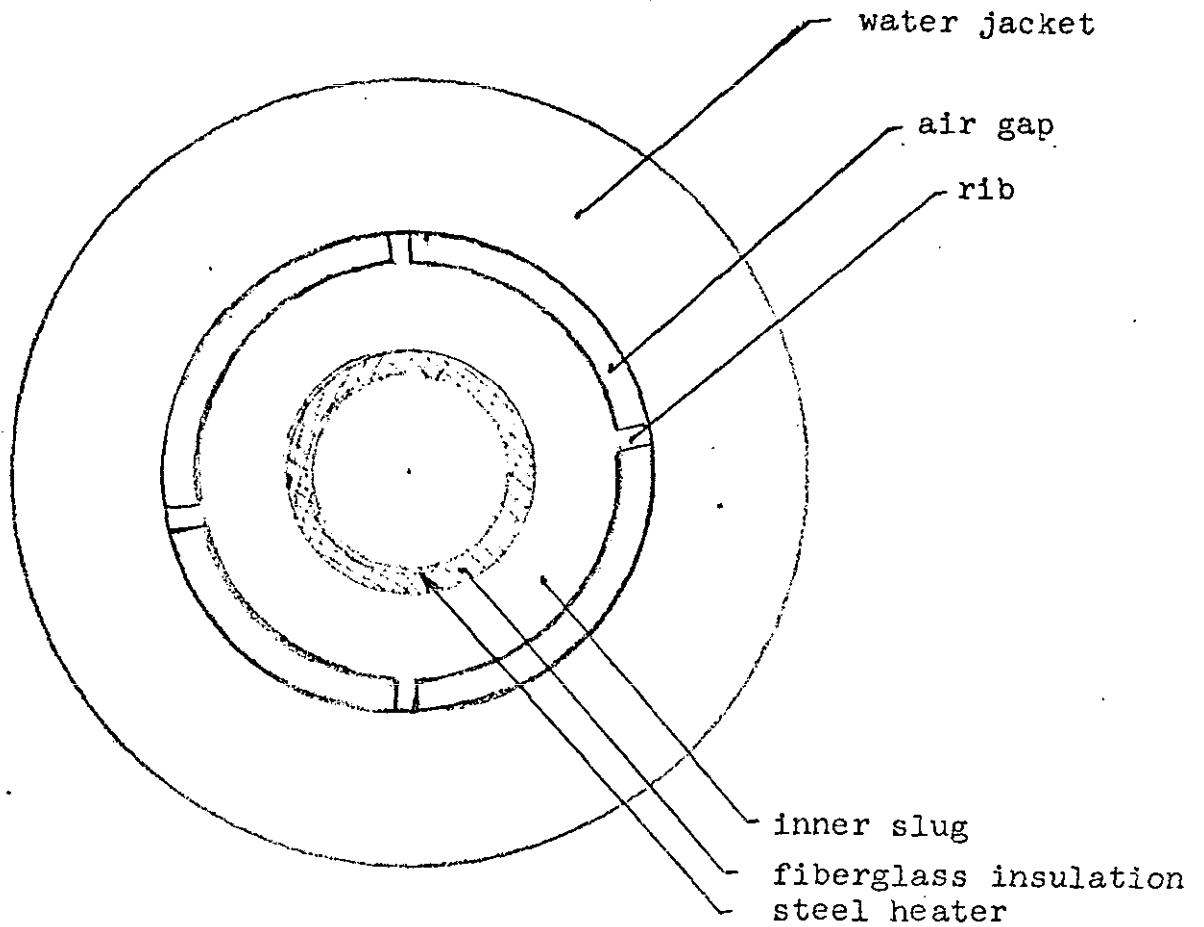


FIGURE 9. Typical Transient Cooling Tests

FIGURE 10

Cross Sectional View of Test Assembly
for Internal Heat Transfer Tests



Dimensions:

Water Jacket		
	OD	4.01 in.
	ID	2.59 in.
Inner Slug		
	OD	2.22 in.
	ID	1.25 in.
Steel Heater		
	OD	1.00 in.
	ID	0.87 in.

FIGURE 11

Schematic of Test Section for Internal Heat Transfer Tests

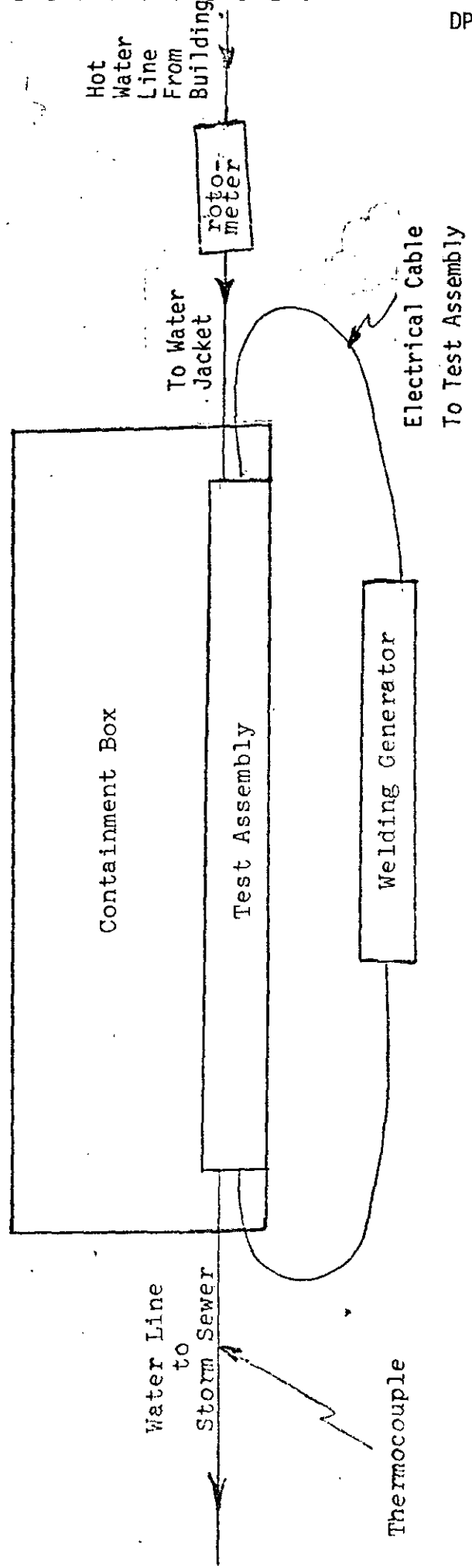


FIGURE 12

Data from Tests for Internal Heat Transfer

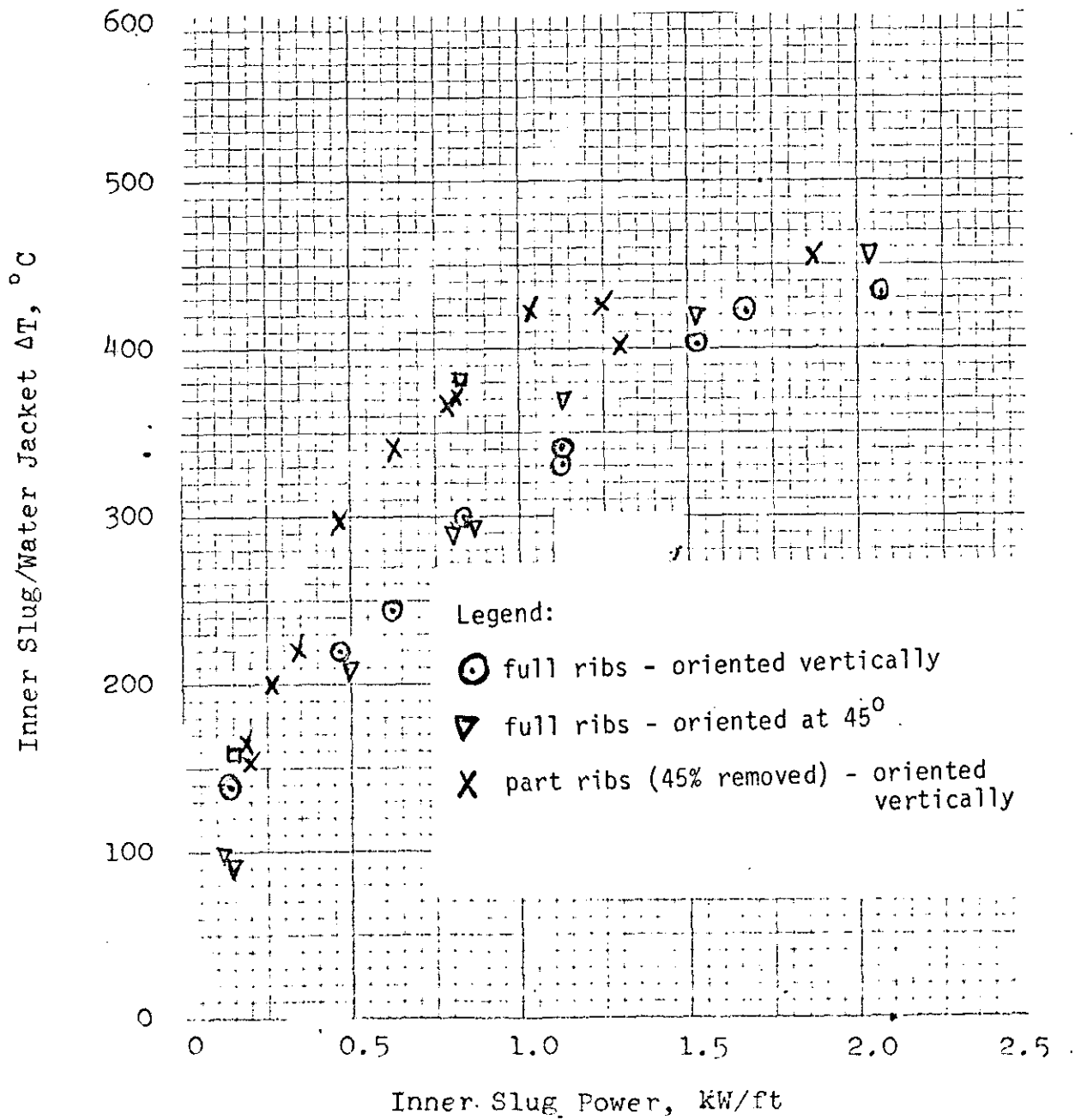


Figure 13: Overall Heat Transfer Coefficient for Rib Conduction

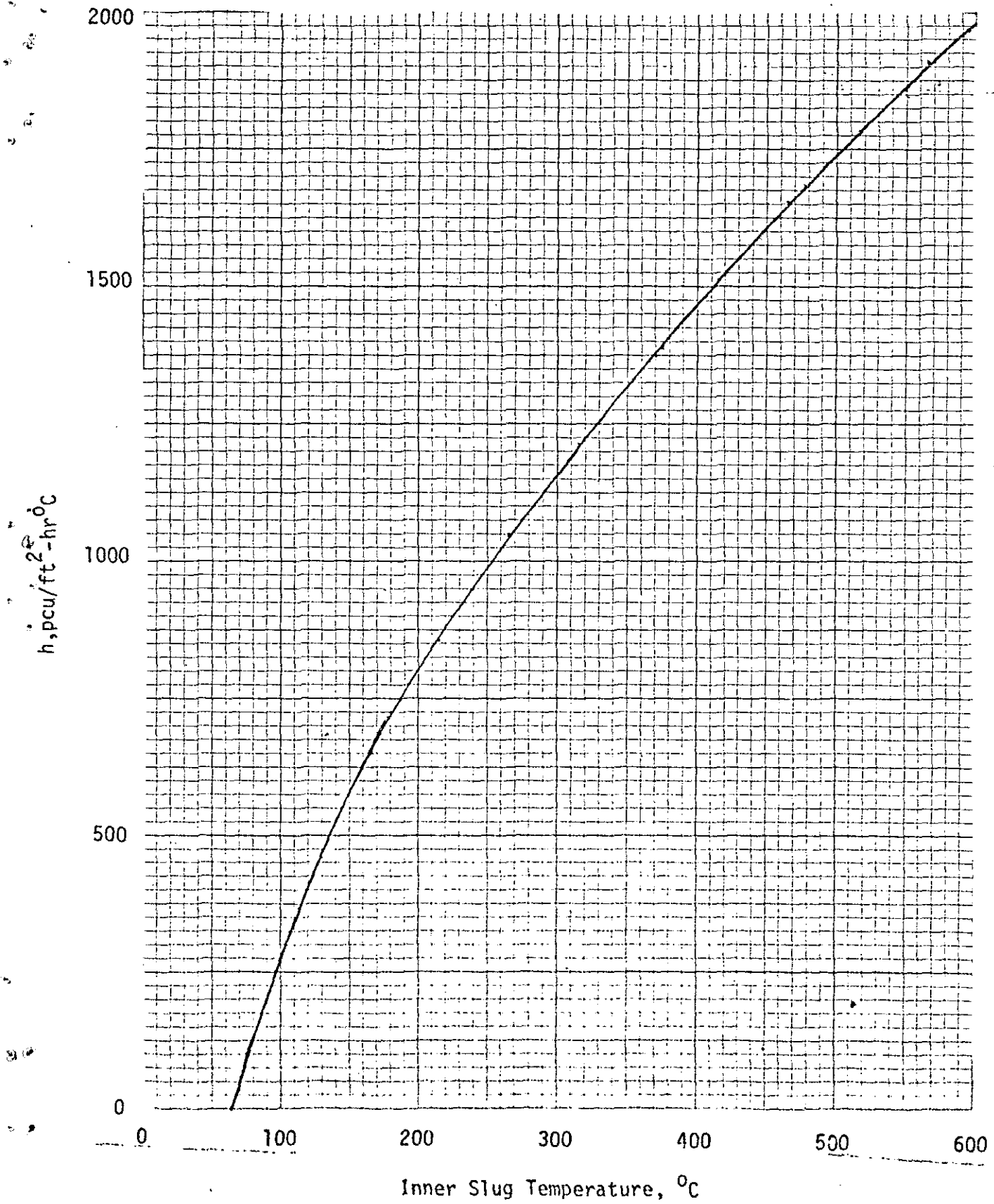
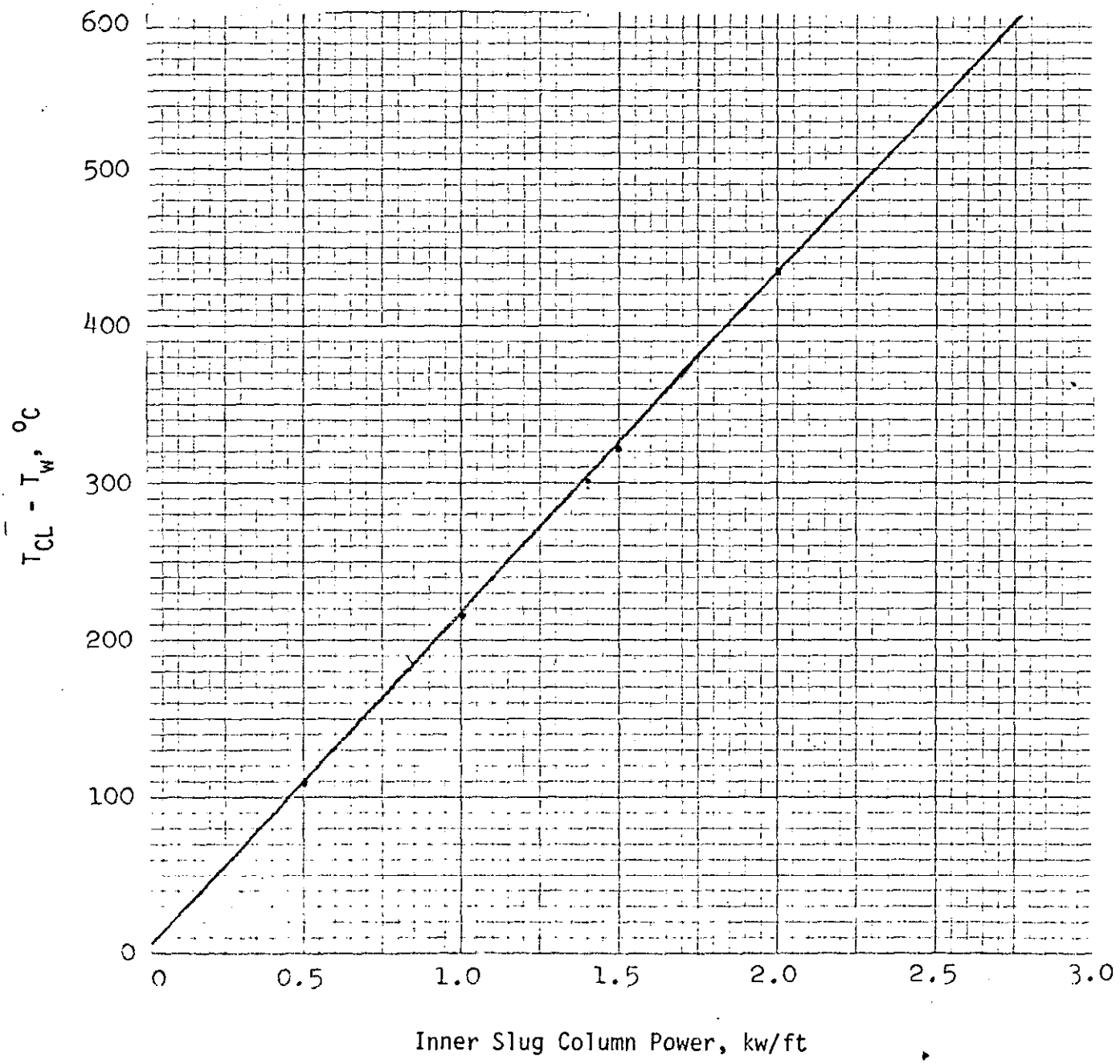


Figure 14

Maximum Outer Slug Temperature in Mark 31A Assemblies From Calculated Gradients (Temperature gradients for other assemblies can be calculated using equations in Appendix A).



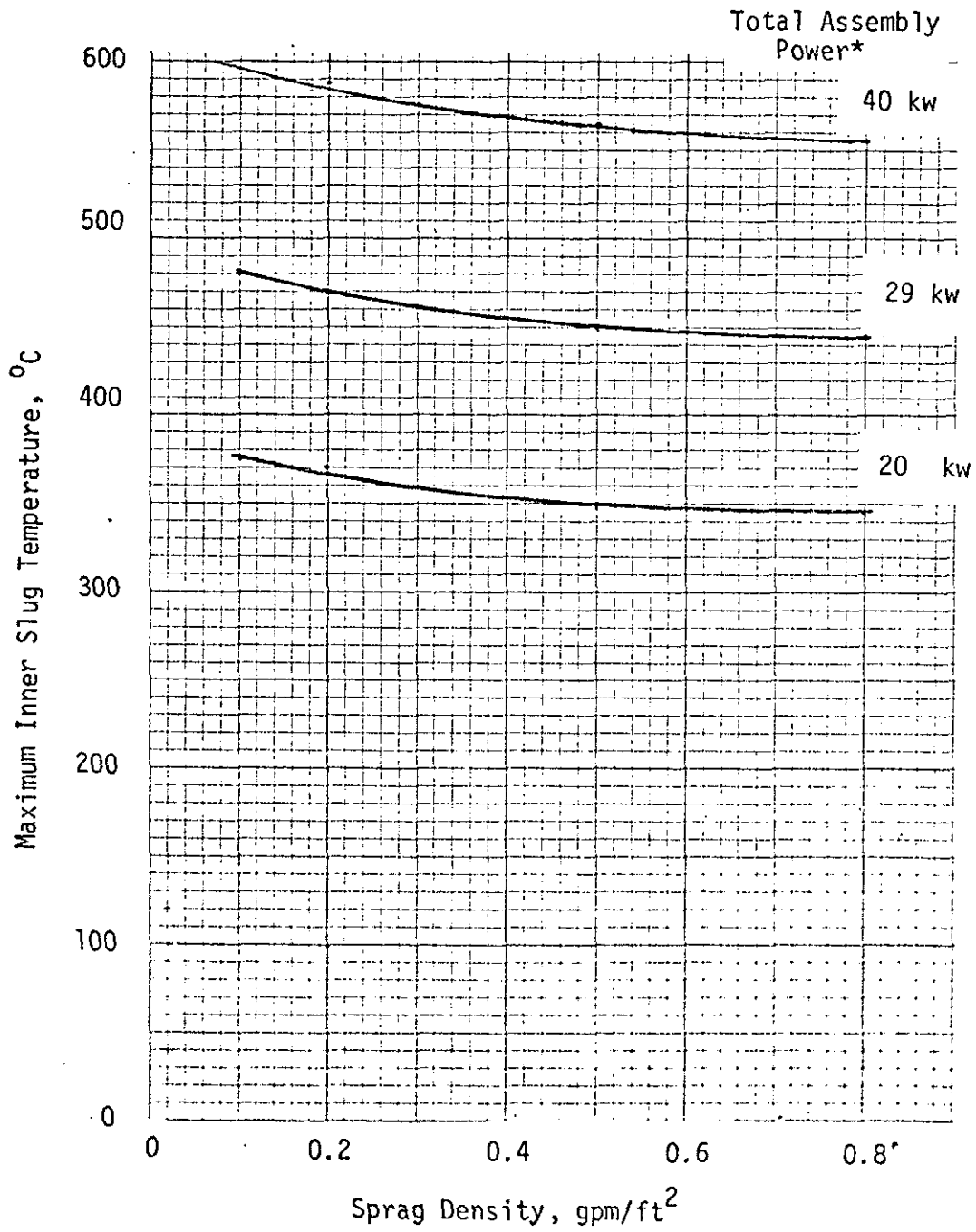
Nomenclature:

T_{CL} = temperature directly beneath the rib centerline (maximum in the outer slug), $^\circ C$

T_W = temperature at the outer surface of the outer slug - assumed invariant with position, $^\circ C$

Figure 15

Calculated Maximum Slug Temperature in Mark 31A Assemblies



* Calculations based on an axial flux peaking of 1.4.

Table ISpray Floor Coverage
P-Area - 12/12/74

	<u>Measured (gpm/ft²)</u>		<u>Required</u>	
	<u>Avg.</u>	<u>Min.</u>	<u>Avg.</u>	<u>Min.</u>
Crane Operating Area (73)	.692	.192	-	.18
Outside Crane Operating (39)	.490	.243	-	.10
All Buckets (112)	.618	.192	.312	-

Table II

Tabulated Data for Internal Heat Transfer

Test*	SLUG TEMPERATURE		GUTLET	INLET	FLOW	VOLTAGE	CURRENT	HEAT GENER.	INNER/OUTER	SLUG	ENERGY
	TC1	TC2	TEMPERATURE	TEMPERATURE	GPM	VOLTS	AMPS	RATE, KW/FT	TEMP. DIFFERENCE	TEMP. DIFFERENCE	BALANCE, %
1A	365.	356.	66.0	56.0	2.4	13.0	520.	0.845	299.5		6.3
2A	280.	275.	61.7	54.5	2.0	9.4	395.	0.464	219.4		-2.4
3A	400.	390.	72.0	54.5	2.0	15.0	600.	1.125	331.8		-2.7
4A	500.	494.	70.5	57.5	4.8	20.7	800.	2.070	433.0		0.5
5A	470.	460.	66.5	57.0	4.8	18.0	670.	1.507	403.3		0.2
6A	490.	480.	67.7	57.0	4.8	19.0	705.	1.674	422.6		-1.2
7A	410.	397.	64.3	57.0	4.8	15.5	580.	1.124	342.8		-2.9
8A	310.	298.	63.5	54.5	2.0	11.0	440.	0.605	245.0		1.8
9A	197.	193.	57.0	54.5	2.0	5.0	225.	0.141	139.3		-17.3
1B	147.	145.	57.0	54.5	2.1	5.0	240.	0.150	90.3		-15.5
2B	437.	434.	71.5	54.5	2.0	15.5	580.	1.124	372.5		0.2
3B	485.	482.	77.0	54.5	2.0	18.0	680.	1.530	417.8		2.9
4B	360.	358.	67.5	54.5	2.0	13.0	510.	0.629	298.0		-3.5
5B	270.	265.	61.0	54.2	2.4	10.0	400.	0.500	209.9		-7.7
6B	525.	515.	70.0	57.5	4.8	21.0	780.	2.047	456.3		3.3
7B	370.	355.	77.0	54.2	2.1	13.2	520.	0.858	296.9		-84.2 **
8B	150.	154.	58.0	54.2	1.8	5.0	230.	0.144	95.9		-57.0 **
1C	250.	259.	58.5	54.0	1.9	8.5	250.	0.266	198.3		-6.2
2C	432.	434.	66.5	54.0	1.9	15.5	420.	0.814	372.8		3.7
3C	465.	465.	75.5	54.0	1.8	20.0	520.	1.300	400.3		1.8
4C	515.	516.	69.0	57.5	4.6	24.2	620.	1.875	452.3		6.9
5C	427.	430.	62.4	57.5	4.8	15.5	410.	0.794	368.5		2.3
6C	355.	359.	61.7	54.0	2.0	11.7	320.	0.468	299.1		-8.6
7C	220.	220.	57.5	54.0	2.1	7.0	210.	0.184	164.3		-32.0 **
8C	205.	215.	57.5	54.0	2.0	7.0	220.	0.192	154.3		-20.0 **
9C	400.	495.	67.0	57.5	4.8	22.0	455.	1.251	425.3		-20.3 **
10C	278.	276.	59.5	57.0	4.8	10.0	285.	0.356	218.8		-11.2 **
11C	470.	400.	61.2	57.5	4.8	14.0	370.	0.647	340.6		9.5
12C	485.	485.	63.5	57.5	4.8	18.0	455.	1.024	424.5		7.2

* Key
 A - Tests with full ribs - oriented vertically.
 B - Tests with full ribs - oriented at 45° to vertical.
 C - Tests with 45% of each rib removed - oriented vertically.

** Probable error in measured flow or temperature. Slug temperature inconsistent with other data taken at similar conditions.

APPENDIX ACALCULATIONS OF TEMPERATURE DISTRIBUTION IN THE
MARK 30A/MARK 31A OUTER SLUGNomenclature

D_o = outer diameter of slug, ft

D_i = inner diameter of slug, ft

δ = 1/2 rib width at tip, ft

β = length of rib per foot of slug length, dimensionless

L = 1/2 arithmetic mean circumference of slug (defined in text), ft

t = total thickness of clad slug, ft

S = distance from outer surface of clad slug to interface between bare slug and inner cladding, ft

ϕ = heat flux through rib, $\text{pcu}/\text{ft}^2\text{-hr}^\circ\text{C}$

K = thermal conductivity of metal, $\text{pcu}/\text{ft-hr}^\circ\text{C}$

T = metal temperature in slug, $^\circ\text{C}$

T_o = outer surface temperature of slug, $^\circ\text{C}$

T' = transformed temperatures (defined in text), $^\circ\text{C}$

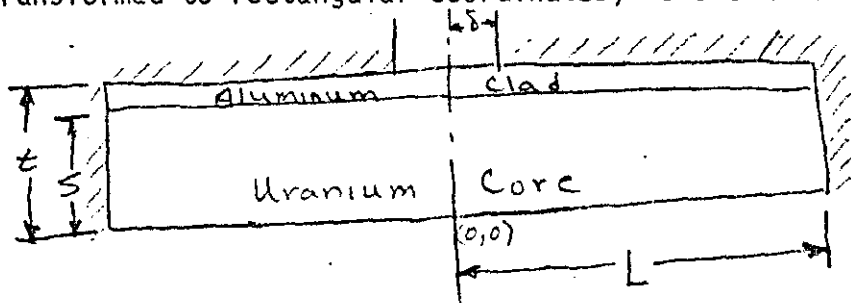
n = a positive integer

Region subscripts/superscripts

I refers to the uranium core (bare slug)

II refers to aluminum cladding

This Appendix summarizes the mathematical analysis used in obtaining temperature distribution in the Mark 30A/Mark 31A outer slug. A sketch of the outer slug (transformed to rectangular coordinates) is shown below:



Adiabatic surfaces represented by hashed lines.

The following approximate transformation equations were used:

$$2L = \pi(D_o + D_i) / 2$$

$$2t = \pi(D_o - D_i)$$

$$\phi = P / 2\beta\delta$$

The following assumptions were used in solving the problem:

- 1) no heat generation in the outer slug
- 2) all heat transferred to the outer slug through a single rib
- 3) constant temperature T_0 at the slug OD ($y = 0$)

The slug is divided into two regions representing the uranium core and the aluminum clad. Under the assumption of zero heat generation in the slug, the governing differential equations are:

$$\nabla^2 T_I = 0 \quad (\text{region I representing the uranium core}) \quad (1A)$$

$$\nabla^2 T_{II} = 0 \quad (\text{region II representing the aluminum clad}) \quad (2A)$$

Analysis is simplified by the following transformation on temperature:

$$\bar{T}(x, y) = T(x, y) - T_0 \quad (3A)$$

Applying this transformation to equations (1A) and (2A):

$$\nabla^2 \bar{T}_I = 0 \quad (4A)$$

$$\nabla^2 \bar{T}_{II} = 0 \quad (5A)$$

Boundary conditions on \bar{T}_I and \bar{T}_{II} are listed below:

$$1) \frac{\partial \bar{T}_I}{\partial x}(0, y) = 0$$

$$2) \frac{\partial \bar{T}_I}{\partial x}(\pm L, y) = 0$$

$$3) \bar{T}_I(x, 0) = 0$$

$$4) \frac{\partial \bar{T}_{II}}{\partial x}(0, y) = 0$$

$$5) \frac{\partial \bar{T}_{II}}{\partial x}(\pm L, y) = 0$$

$$6) \frac{\partial \bar{T}_{II}}{\partial y}(x, \pm \delta) = \begin{matrix} -\phi/k_{II}, & |x| < \delta \\ 0, & |x| > \delta \end{matrix}$$

$$7) \bar{T}_I(x, S) = \bar{T}_{II}(x, S)$$

$$8) -K_I \frac{\partial \bar{T}_I}{\partial y}(x, S) = -K_{II} \frac{\partial \bar{T}_{II}}{\partial y}(x, S)$$

-A4-

Equations (4A) and (5A) can be solved by separation of variables to give the following candidate solutions:

$$\bar{u}_I(x, y) = \sum_1^{\infty} (a_n^I \sin \alpha_n^I x + b_n^I \cos \alpha_n^I x) (C_n^I \sinh \alpha_n^I y + D_n^I \cosh \alpha_n^I y) \quad (6A)$$

$$\bar{u}_{II}(x, y) = \sum_1^{\infty} (a_n^{II} \sin \alpha_n^{II} x + b_n^{II} \cos \alpha_n^{II} x) (C_n^{II} \sinh \alpha_n^{II} y + D_n^{II} \cosh \alpha_n^{II} y) \quad (7A)$$

where α_n 's, a_n 's, b_n 's, c_n 's, and d_n 's are to be determined from the boundary conditions on τ as summarized below:

$$\text{B. C. 1 - } \frac{\partial \bar{u}_I}{\partial x}(0, y) = 0$$

Evaluating the partial derivative of $\tau_I(x, y)$ with respect to x at $x = 0$ gives:

$$\sum_1^{\infty} \alpha_n^I a_n^I (C_n^I \sinh \alpha_n^I y + d_n^I \cosh \alpha_n^I y) = 0$$

which can be true for all y whenever $a_n^I = 0$ or $\alpha_n^I = 0$. But $\alpha_n^I = 0$ yields a trivial solution, thus the first boundary condition requires that

$$a_n^I = 0$$

$$\text{B. C. 2 - } \frac{\partial \bar{u}_I}{\partial x}(\pm L, y) = 0$$

(8A)

Evaluating $\frac{\partial \bar{u}_I}{\partial x}$ at $x = +L$ gives:

$$\sum_1^{\infty} \alpha_n^I (a_n^I \cos \alpha_n^I L - b_n^I \sin \alpha_n^I L) (C_n^I \sinh \alpha_n^I y + D_n^I \cosh \alpha_n^I y)$$

But from (8A), $a_n^I = 0$...

$$- \sum_1^{\infty} \alpha_n^I b_n^I \sin \alpha_n^I L (C_n^I \sinh \alpha_n^I y + d_n^I \cosh \alpha_n^I y) = 0$$

This can be true for all y whenever:

$$\alpha_n^I = 0$$

(a trivial solution)

$$b_n^I = 0$$

(a trivial solution since $a_n^I = 0$)

$$\sin \alpha_n^I L = 0$$

Thus the second boundary condition requires that

$$\sin \alpha_n^I L = 0$$

This condition is satisfied if and only if

$$\alpha_n^I L = n\pi$$

or

$$\alpha_n^I = \frac{n\pi}{L}$$

(9A)

B. C. 3 - $\bar{z}(x, 0) = 0$

Evaluating $\tau(x, y)$ at $y = 0$ and making use of equations (8A) and (9A):

$$\sum_1^{\infty} b_n^I \cos \frac{n\pi x}{L} d_n^I = 0$$

Because b_n^I cannot be zero, boundary condition 3 requires that

$$d_n^I = 0$$

(10A)

B. C. 4 - $\frac{\partial \bar{z}^{II}}{\partial x}(0, y) = 0$

The same analysis used in applying the first boundary condition can be used to derive:

$$a_n^{II} = 0$$

(11A)

-A6-

$$\text{B. C. 5 - } \frac{\partial \bar{z}_{II}}{\partial x}(\pm L, y) = 0$$

Applying the same logic as for B. C. 2

$$\alpha_n^{II} = \alpha_n^I = \frac{n\pi}{L}$$

(12A)

At this point it is convenient to rewrite equations (6A) and (7A) making use of the information derived in equations (8A) through (12A).

$$\bar{z}_I(x, y) = \sum_1^{\infty} b_n^I \cos \frac{n\pi x}{L} C_n^I \sinh \frac{n\pi y}{L} \quad (13A)$$

$$\bar{z}_{II}(x, y) = \sum_1^{\infty} b_n^{II} \cos \frac{n\pi x}{L} \left(C_n^{II} \sinh \frac{n\pi y}{L} + D_n^{II} \cosh \frac{n\pi y}{L} \right) \quad (14A)$$

Furthermore, notation can be simplified by the following definitions:

Let:

$$A_n = b_n^I C_n^I$$

$$B_n = b_n^{II} C_n^{II}$$

$$C_n = b_n^{II} D_n^{II}$$

Then,

$$\bar{z}_I(x, y) = \sum_1^{\infty} A_n \cos \frac{n\pi x}{L} \sinh \frac{n\pi y}{L} \quad (15A)$$

$$\bar{z}_{II}(x, y) = \sum_1^{\infty} \cos \frac{n\pi x}{L} \left(B_n \sinh \frac{n\pi y}{L} + C_n \cosh \frac{n\pi y}{L} \right) \quad (16A)$$

-A7-

$$\text{B. C. 6 - } \frac{\partial \bar{z}_{II}}{\partial y}(x, t) = \begin{cases} -\frac{\delta}{K}, & |x| < \delta \\ 0, & |x| > \delta \end{cases}$$

A Fourier series expansion can be found in reference 5 for the following function:

$$f(\xi) = \frac{c}{l} + \frac{2}{\pi} \sum_1^{\infty} \frac{(-1)^n}{n} \sin \frac{n\pi c}{l} \cos \frac{n\pi \xi}{l}$$

where,

$$f(\xi) = \begin{cases} 0, & 0 < \xi < l-c \\ 1, & l-c < \xi < l+c \\ 0, & l+c < \xi < 2l \end{cases}$$

if the variable ξ is transformed by

$$\xi = l + x$$

then

$$f(x) = \frac{c}{l} + \frac{2}{\pi} \sum_1^{\infty} \frac{(-1)^n}{n} \sin \frac{n\pi c}{l} \cos \left(n\pi + \frac{n\pi x}{l} \right) \quad (17A)$$

where

$$f(x) = \begin{cases} 0, & |x| < c \\ 1, & |x| > c \end{cases}$$

Equation (17A) can be simplified to

$$f(x) = \frac{c}{l} + \frac{2}{\pi} \sum_1^{\infty} \frac{1}{n} \sin \frac{n\pi c}{l} \cos \frac{n\pi x}{l}$$

Now if c and l are chosen such that

$$c = \delta$$

$$l = L$$

then B. C. 6 can be written

$$\frac{\partial \bar{z}_{II}}{\partial y}(x, t) = -\frac{\delta}{K_{II}} f(x) = -\frac{\delta}{LK_{II}} - \frac{2\delta}{\pi K_{II}} \sum_1^{\infty} \frac{1}{n} \sin \frac{n\pi \delta}{L} \cos \frac{n\pi x}{L}$$

(Note: that δ is negative as a result of the sign convention chosen in setting up the problem, so that $-\delta$ is positive.)

It is convenient at this point to use the following approximation:

Because $\delta/L \ll 1$...

$$\frac{\partial \bar{z}_{II}}{\partial y}(x, t) \approx -\frac{2\delta}{\pi k_{II}} \sum_1^{\infty} \frac{1}{n} \sin \frac{n\pi\delta}{L} \cos \frac{n\pi x}{L} \quad (18A)$$

This approximation will be circumvented later in the development to return the original rigor to the solution.

Evaluating $\frac{\partial \bar{z}_{II}}{\partial y}$ at $y = t$ and using equation (18A) results in:

$$\sum_1^{\infty} \frac{n\pi}{L} \cos \frac{n\pi x}{L} (B_n \cosh \frac{n\pi t}{L} + C_n \sinh \frac{n\pi t}{L}) = -\frac{2\delta}{k_{II}} \sum_1^{\infty} \sin \frac{n\pi\delta}{L} \cos \frac{n\pi x}{L}$$

$$\sum_1^{\infty} \cos \frac{n\pi x}{L} \left[\frac{n\pi}{L} (B_n \cosh \frac{n\pi t}{L} + C_n \sinh \frac{n\pi t}{L}) + \frac{2\delta}{k_{II}} \sin \frac{n\pi\delta}{L} \right] = 0$$

This implies that

$$\frac{n\pi}{L} (B_n \cosh \frac{n\pi t}{L} + C_n \sinh \frac{n\pi t}{L}) + \frac{2\delta}{k_{II}} \sin \frac{n\pi\delta}{L} = 0$$

from which

$$C_n = -\frac{2\delta L}{n^2 \pi^2 k_{II}} \frac{\sin \frac{n\pi\delta}{L}}{\sinh \frac{n\pi t}{L}} - \frac{B_n}{\tanh \frac{n\pi t}{L}} \quad (19A)$$

$$\text{B. C. 7 - } \bar{z}_I(x, s) = \bar{z}_{II}(x, s)$$

Evaluating τ_I and τ_{II} at $y = s$ yields

$$\sum_1^{\infty} A_n \cos \frac{n\pi x}{L} \sinh \frac{n\pi s}{L} = \sum_1^{\infty} \cos \frac{n\pi x}{L} (B_n \sinh \frac{n\pi s}{L} + C_n \cosh \frac{n\pi s}{L})$$

which implies that

$$A_n = B_n + \frac{C_n}{\tanh \frac{n\pi s}{L}} \quad (20A)$$

-A9-

$$\text{B. C. 8 - } \frac{-K_I \frac{\partial \bar{c}_I}{\partial y}(x, s)}{-K_{II} \frac{\partial \bar{c}_{II}}{\partial y}(x, s)}$$

Evaluating $\frac{\partial \bar{c}_I}{\partial y}$ and $\frac{\partial \bar{c}_{II}}{\partial y}$ at $y = s$ yields

$$-K_I \sum_1^{\infty} \frac{n\pi}{L} A_n \cos \frac{n\pi x}{L} \cosh \frac{n\pi s}{L} = -K_{II} \sum_1^{\infty} \frac{n\pi}{L} \cos \frac{n\pi x}{L} (B_n \cosh \frac{n\pi s}{L} + C_n \sinh \frac{n\pi s}{L})$$

$$-\sum_1^{\infty} \frac{n\pi}{L} \cos \frac{n\pi x}{L} (K_I A_n \cosh \frac{n\pi s}{L} - K_{II} B_n \cosh \frac{n\pi s}{L} - K_{II} C_n \sinh \frac{n\pi s}{L}) = 0$$

which implies that

$$K_I A_n \cosh \frac{n\pi s}{L} = K_{II} (B_n \cosh \frac{n\pi s}{L} + C_n \sinh \frac{n\pi s}{L})$$

from which,

$$A_n = \frac{K_{II}}{K_I} (B_n + C_n \tanh \frac{n\pi s}{L}) \quad (21A)$$

At this point all boundary conditions have been applied and the problem reduced to solving three linear equations in three unknown, viz. equations (19A, 20A, and 21A). The solution to these equations is:

$$B_n = \frac{-2\delta L}{n^2 \pi^2 K_{II}} \frac{\sin n\pi \delta / L}{\sinh n\pi t / L} \quad (22A)$$

$$\frac{1}{\tanh n\pi t / L} + \frac{(1 - K_{II}/K_I) \tanh n\pi s / L}{K_{II}/K_I \tanh^2 n\pi s / L - 1}$$

$$C_n = \frac{-2\delta L}{n^2 \pi^2 K_{II}} \frac{\sin n\pi \delta / L}{\sinh n\pi t / L} - \frac{B_n}{\tanh n\pi t / L} \quad (23A)$$

$$A_n = B_n + \frac{C_n}{\tanh n\pi s / L} \quad (24A)$$

It is possible to circumvent the approximation that $\delta/L \ll 1$ used in deriving equation (18A) for

$$\frac{\partial \bar{c}_{II}}{\partial y}(x, t)$$

Define a variable $\Gamma(x,y)$ such that

$$\Gamma_I(x,y) = \bar{z}_I(x,y) + a_1 y + b_1 \quad (25A)$$

$$\Gamma_{II}(x,y) = \bar{z}_{II}(x,y) + a_2 y + b_2 \quad (26A)$$

Note that

$$\nabla^2 \Gamma_I = 0$$

$$\nabla^2 \Gamma_{II} = 0$$

Thus if Γ_I and Γ_{II} can be made to satisfy the eight boundary conditions of our problem, the temperature distribution inside the slug can be written in terms of these variables.

B. C. 1 and B. C. 2

Note that $\frac{\partial \Gamma_I}{\partial x} = \frac{\partial \bar{z}_I}{\partial x}$ so that boundary conditions 1) and 2) are both satisfied by Γ_I .

B. C. 3

$$\Gamma_I(x,0) = \bar{z}_I(x,0) + b_1$$

But $\tau_I(x,0) = 0$

Thus, if $\Gamma_I(x,0) = 0$

(27A)

$$b_1 = 0$$

B. C. 4 and B. C. 5

Note that $\frac{\partial \Gamma_{II}}{\partial x} = \frac{\partial \bar{z}_{II}}{\partial x}$ so that boundary conditions 4) and 5) are satisfied by Γ_{II} .

-A11-

B. C. 6

$$\frac{\partial \Gamma_I}{\partial y}(x, t) = \frac{\partial \bar{z}_I}{\partial y}(x, t) + a_2 \quad (28A)$$

But note that

$$\frac{\partial \bar{z}_I}{\partial y}(x, t) = -\frac{z\delta}{\pi k_{II}} \sum_1^{\infty} \frac{1}{n} \sin \frac{n\pi\delta}{L} \cos \frac{n\pi x}{L} \quad (29A)$$

and B. C. 6 requires that

$$\frac{\partial \Gamma_I}{\partial y}(x, t) = -\frac{z\delta}{k_{II}L} - \frac{z\delta}{\pi k_{II}} \sum_1^{\infty} \frac{1}{n} \sin \frac{n\pi\delta}{L} \cos \frac{n\pi x}{L} \quad (30A)$$

Substitution of (29A) into (30A) yields:

$$\frac{\partial \Gamma_I}{\partial y}(x, t) = -\frac{z\delta}{k_{II}L} + \frac{\partial \bar{z}_I}{\partial y}(x, t) \quad (31A)$$

Comparing equations (31A) and (28A) shows:

$$a_2 = -\frac{z\delta}{k_{II}L} \quad (32A)$$

B. C. 7

$$\Gamma_I(x, s) = \bar{z}_I(x, s) + a_1 s + b_1$$

$$\Gamma_{II}(x, s) = \bar{z}_{II}(x, s) + a_2 s + b_2$$

Now if $\Gamma_I(x, s) = \Gamma_{II}(x, s)$; then

$$\bar{z}_I(x, s) + a_1 s + b_1 = \bar{z}_{II}(x, s) + a_2 s + b_2$$

but τ_I and τ_{II} are so defined that

$$\bar{z}_I(x, s) = \bar{z}_{II}(x, s)$$

-A12-

Then,

$$a_1 s + b_1 = a_2 s + b_2$$

or since $b_1 = 0$

$$a_1 s = a_2 s + b_2$$

(33A)

B.C. 8

$$-K_I \frac{\partial \Gamma_I}{\partial y}(x, s) = -K_I \frac{\partial \bar{z}_I}{\partial y}(x, s) - K_I a_1$$

$$-K_{II} \frac{\partial \Gamma_{II}}{\partial y}(x, s) = -K_{II} \frac{\partial \bar{z}_{II}}{\partial y}(x, s) - K_{II} a_2$$

Then,

$$-K_I \frac{\partial \bar{z}_I}{\partial y}(x, s) - K_I a_1 = -K_{II} \frac{\partial \bar{z}_{II}}{\partial y}(x, s) - K_{II} a_2$$

From which,

$$a_1 = \frac{K_{II}}{K_I} a_2$$

(34A)

Note then that Γ_I and Γ_{II} can be made to satisfy all eight boundary conditions exactly whenever equations (32A) through (34A) are met and $b_1 = 0$. Furthermore, equations (32A) through (34A) are satisfied by the following equations:

$$a_2 = -\frac{2\theta\delta}{K_{II}L} \quad (35A)$$

$$a_1 = -\frac{2\theta\delta}{K_I L} \quad (36A)$$

$$b_2 = -\frac{2\theta\delta}{L} \left(\frac{s}{K_I} - \frac{s}{K_{II}} \right) \quad (37A)$$

Thus solutions to the differential equations (1A) and (2A) which satisfy the boundary conditions 1) - 8) are

$$T_I(x, y) = T_0 - \frac{2\theta\delta y}{K_I L} + \sum_1^{\infty} A_n \cos \frac{n\pi x}{L} \sinh \frac{n\pi y}{L}$$

$$T_{II}(x, y) = T_0 - \frac{2\theta\delta}{L} \left(\frac{y-s}{K_{II}} + \frac{s}{K_I} \right) + \sum_1^{\infty} \cos \frac{n\pi x}{L} \left(B_n \sinh \frac{n\pi y}{L} + D_n \cosh \frac{n\pi y}{L} \right)$$

where the A_n 's, B_n 's, and C_n 's are given by equations (22A) through (24A).